MATERIALS SCIENCE

A "cation-anion regulation" synergistic anode host for dendrite-free lithium metal batteries

Weidong Zhang,[1,2] Houlong L. Zhuang,[3] Lei Fan,[1,2] Lina Gao,[4] Yingying Lu[1,2]*

Dendritic Li deposition has been "a Gordian knot" for almost half a century, which significantly hinders the practical use of high-energy lithium metal batteries (LMBs). The underlying mechanisms of this dendrite formation are related to the preferential lithium deposition on the tips of the protuberances of the anode surface and also associated with the concentration gradient or even depletion of anions during cycling. Therefore, a synergistic regulation of cations and anions at the interface is vital to promoting dendrite-free Li anodes. An ingenious molecular structure is designed to realize the "cation-anion regulation" with strong interactions between adsorption sites and ions at the molecular level. A quaternized polyethylene terephthalate interlayer with a "lithiophilic" ester building block and an "anionphilic" quaternary ammonium functional block can guide ions to form dendrite-free Li metal deposits at an ultrahigh current density of 10 mA cm^{-2}, enabling stable LMBs.

INTRODUCTION

Lithium metal is regarded as an ultimate anode material because of its ultrahigh theoretical specific capacity (3861 mA·hour g^{-1} or 2061 mA·hour cm^{-3}) and extremely low electrochemical potential (−3.04 V versus standard hydrogen electrode) (*1*). However, batteries that use lithium metal have suffered from great safety hazards for almost half a century. Uncontrolled proliferation of uneven Li deposition during cycling is the main source of internal short circuiting or even explosion hazards (*2*, *3*). Early in the 1990s, NEC and Mitsui carried out confirmation tests on more than 500,000 lithium metal batteries (LMBs) to figure out the complicated Li metal chemistry, but failed after 2 years of hard work (*4*, *5*). Recently, with the rapid development of electrical devices and explosive demand for high-energy rechargeable batteries, researchers have regained confidence in the revivification of Li metal anodes. Many efforts have been devoted to suppressing the lithium dendrites or even developing a dendrite-free lithium anode for practical applications of high-energy LMBs, including Li-S and Li-air batteries (*6*–*8*).

The failure mechanism of LMBs is controversial and complicated. It could involve mass transfer and diffusion of ions, electrochemical reaction kinetics, electrolyte/electrode interface build and break, and so on (*9*, *10*). The prevailing understanding is that lithium dendrite growth is a result of joint actions with multiple mechanisms (*11*). When a cell is charged at a fixed current density, Li-ion flux is more concentrated on the tip of the rough lithium substrate due to the enhanced local current density, known as the "tip effect" (Fig. 1A, Li depositing process) (*12*, *13*). The unavoidable defects of the electrode surface, either from the rupture of solid electrolyte interphases (SEIs) or nonuniformity during the manufacturing process, can be the dendrite nucleation seeds and trigger the growth of dendrites (*14*). On further deposition of the nuclei, the roughness of the interface amplifies and that of the dendrite proliferates. Meanwhile, anions are expelled by the electric field during polarization (Fig. 1A, Li depositing process) and will deplete near the negative electrode. A large electric field called "space charge" is created near the electrode/electrolyte interface, which is known as another source of uncontrolled deposition of lithium (*11*, *15*). Theoretical research confirms that the dendrites will grow at a velocity equal to $-\mu_a E_0$ (where μ_a is the mobility of anion and E_0 is the electric field) (*16*).

Various materials have been developed in response to the proposed failure mechanisms. (i) Homogenizing Li-ion flux: Using materials with polar functional groups (that is, N, O, and S) can attract large amounts of Li ions, regulate their distribution at the anode interface, and promote uniform lithium deposition. For example, a three-dimensional (3D) oxidized polyacrylonitrile nanofiber (*17*) or glass fiber (*18*) used as a buffer interlayer near the anode surface can interact with lithium ions because of their high binding energies with polar groups. This interaction effectively undermines the preferential distribution of lithium ions, aiding flat electrodeposition. These kinds of materials exhibit a "lithiophilic" affinity. (ii) Reducing the mobility of anions: As mentioned above, there is a positive correlation between the lithium dendrite growth rate and the velocity of the anion mobility. If the anions are partially or fully fixed and are immobile during cycling, then the anion concentration gradient can be effectively undermined and the space charge–induced dendritic Li growth can be relieved consequently (*19*, *20*). A series of hybrid electrolytes such as sulfonate salts based on Nafion (*21*) or organic-inorganic electrolyte additives (*22*, *23*) have been created to serve as reservoirs for anions and realized stable Li deposition in many experimental studies. These kinds of materials present an "anionphilic" interaction. (iii) Artificial SEI fabrication: SEIs formed on the highly reactive lithium metal surface usually exhibit poor mechanical strength and heterogeneous interfacial transport properties, both of which can accelerate the growth of Li dendrites. Electrolyte additives such as lithium nitrate ($LiNO_3$) (*24*), lithium halides (that is, LiF, LiCl, and LiBr) (*25*–*27*), and lithium polysulfide (*28*, *29*) can facilitate favorable SEI formation with uniform morphology and chemistry.

Inspired by the binary cooperative molecular systems in nature (*30*), we rationalized material design with both lithiophilicity and anionphilicity at the molecular level, which is able to regulate cation distribution and undermine the anion concentration gradient simultaneously. A dendrite-free lithium anode can be realized under such a synergistic effect of "cation-anion regulation." Here, a quaternized polyethylene terephthalate (q-PET) nonwoven fabric is used as a multifunctional interlayer to host the Li metal to achieve homogenized transport of cations and anions synergistically at the electrode/electrolyte interface and promote a dendrite-free lithium metal anode. q-PET is designed to accommodate ion flux cataclysm with a lithiophilic ester building block and an anionphilic quaternary ammonium functional block,

[1]College of Chemical and Biological Engineering, Zhejiang University, Hangzhou 310027, China. [2]State Key Laboratory of Chemical Engineering, Institute of Pharmaceutical Engineering, Zhejiang University, Hangzhou 310027, China. [3]School for Engineering of Matter, Transport and Energy, Arizona State University, Tempe, AZ 85287, USA. [4]Department of Chemistry, Zhejiang University, Hangzhou 310027, China.
*Corresponding author. Email: yingyinglu@zju.edu.cn

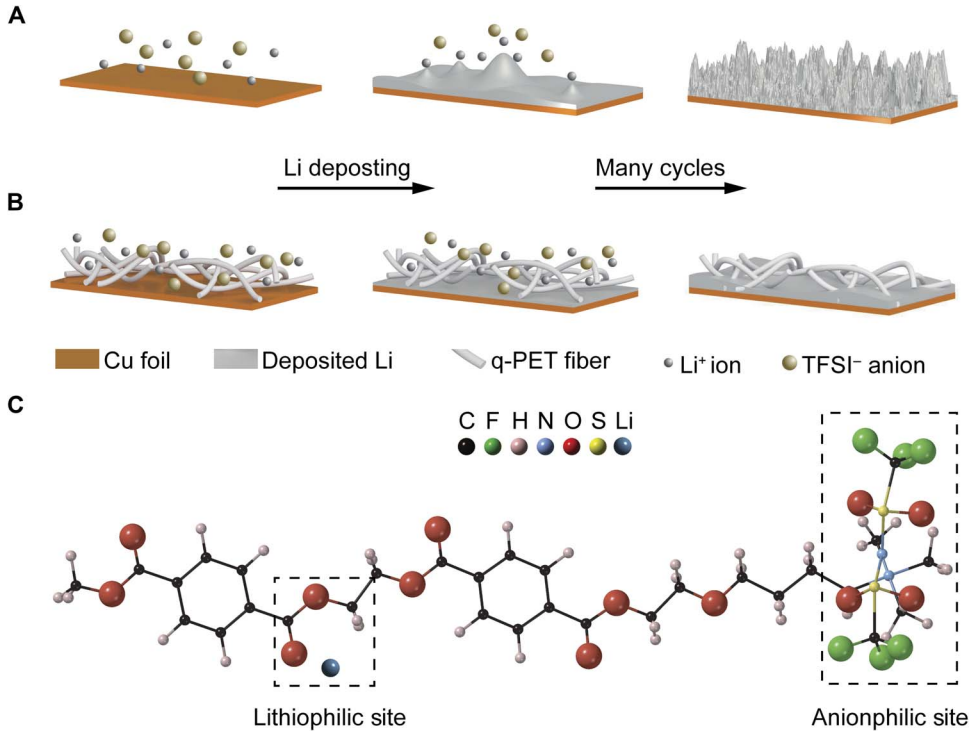

Fig. 1. Schematic illustration of electrodeposition behaviors and synergistic effect at the molecular level. (**A**) Lithium deposition on a routine copper foil. Li-ion flux is more concentrated on the dendrite tip, and the concentration of anions drops near the anode surface, resulting in self-enhanced dendrite growth on repeated cycling. (**B**) Lithium deposition on q-PET interlayer/Cu. q-PET can attract large quantities of Li ions and bis(trifluoromethanesulfonyl)imide (TFSI) anions from its polar functional groups. Uniform ion distribution at the anode surface promotes smooth deposition. (**C**) Sketch of the structure of q-PET. Dendrite-free Li deposition is facilitated via rationally engineered binding toward both Li cation and TFSI anion.

which can serve as ion reservoirs for both cations and anions. As represented in Fig. 1C, the polar ester functional groups in the backbone of q-PET can adhere many Li ions and regulate the Li-ion flux at the electrode interface during lithium plating, relieving the tip effect induced by the unavoidable roughness. Moreover, the quaternary ammonium functional group tethered on the PET molecular skeleton can bind and immobilize a certain amount of anions (that is, $TFSI^-$ and PF_6^-) in the electrolyte, preventing the space charge–induced dendrite formation by a local deficit of anions. On the other hand, quaternary ammonium chloride salt can interact with lithium salt and spontaneously form lithium chloride via an ion exchange reaction (*31*). LiCl was proved as a favorable SEI compound for a stable lithium metal anode (*25*). Considering all these merits in a single structure, the effectiveness of the q-PET/Li composite anode as an alternative choice to the bare lithium metal anode is extensively studied.

RESULTS

Binding energies using density functional theory calculations

We first verified the subtle interactions of q-PET with both lithium cations and TFSI anions, which might play a critical role in uniforming Li deposition. To provide a quantitative description, we performed density functional theory (DFT) calculations using the Vienna Ab initio Simulation Package (see the Supplementary Materials for computational details). We computed the binding energy E_b of TFSI anion interacting with q-PET, defined as the energy difference between the total energies of TFSI anion E_{TFSI} and q-PET $E_{q\text{-}PET}$, that is, $E_b = E_{TFSI} + E_{q\text{-}PET} - E_{TFSI+q\text{-}PET}$. Here, $E_{TFSI+q\text{-}PET}$ refers to the total energy of the hybrid system consisting of both TFSI anion and q-PET. The equation shows that the stronger binding interactions are represented by the more positive binding energy. We found that the calculated E_b is 3.93 eV, which is sufficiently large to imply the strong binding of TFSI anion with q-PET. We also calculated the binding energy between a Li ion and q-PET, and the binding energy E_b is 0.69 eV, which is considerably larger than the binding energy between a Li ion and a commercial polypropylene (PP) separator (fig. S1). We found that the corresponding binding energy is negative ($E_b = -0.35$ eV), suggesting repulsive Coulomb interactions caused by the saturated bonds in the skeleton of PP. Through DFT calculations (summarized in table S1), it is proved that q-PET can provide effective bonding sites for both Li cations and TFSI anions. In the skeleton of q-PET (Fig. 1C), the ester group serves as a lithiophilic site and quaternary ammonium acts as an anionphilic site, attracting both Li ion and TFSI anion.

Materials characterizations

The q-PET fabric exists in a nonwoven micrometer fiber structure with an average fiber diameter of 10 μm (Fig. 2A). q-PET fibers are interlaced and form a staggered overlapping network, which is also confirmed by optical microscopy (fig. S2). The functional interlayer with multitudinous void spaces can increase the electrolyte uptake, facilitating the homogeneous distribution of electrolytes near the anode. Energy-dispersive x-ray spectroscopy (EDX) analysis and elemental EDX maps (figs. S3 and S4) demonstrate the coexistence and homogenous dispersion of carbon, oxygen, nitrogen, and chlorine on the surface

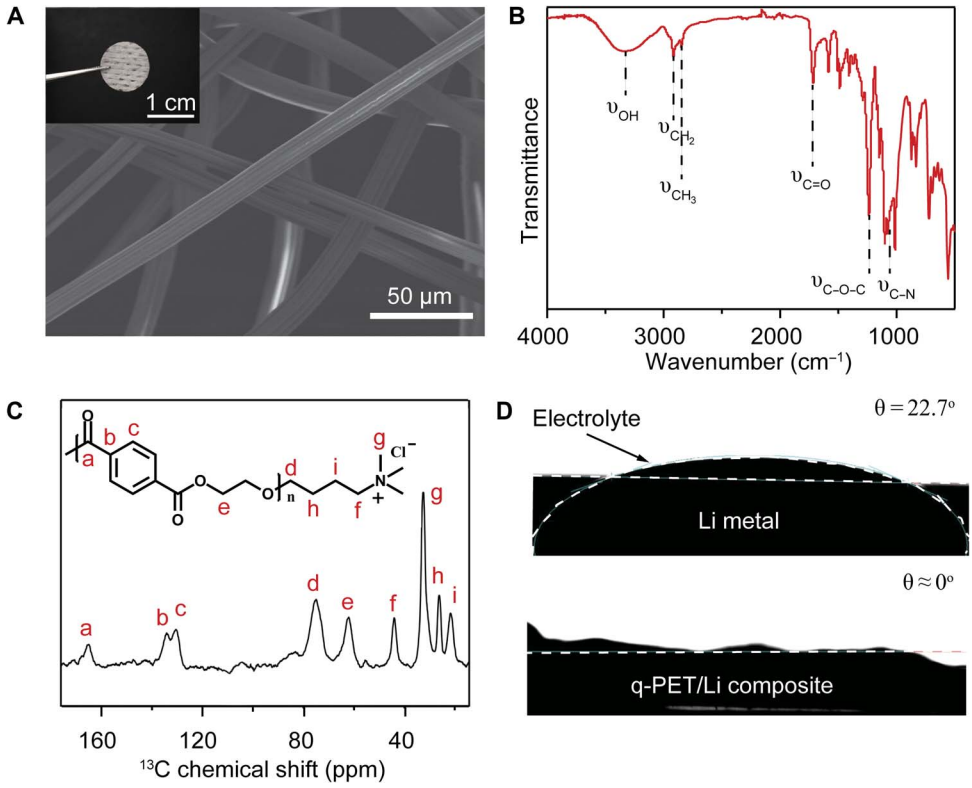

Fig. 2. Surface pictures and characterization of q-PET. (**A**) The q-PET fabric was first cut into the circular layer (inset digital picture), and scanning electron microscopy (SEM) image shows the nonwoven q-PET fiber network. (**B**) FTIR spectrum of q-PET. (**C**) Solid-state ^{13}C CP/MAS NMR spectra of q-PET. (**D**) Contact angles of ether-based electrolytes on bare lithium metal or q-PET/Li composite electrode.

of the q-PET fiber, which agrees well with the expected chemical composition of q-PET. To quantify the element content in the q-PET fiber, elemental analysis using the Dumas combustion method was carried out. The combustion experiment shows that the nitrogen content is 0.52 weight % (wt %), which further verifies the existence of the anionphilic quaternary ammonium function group (table S2).

Fourier transform infrared spectrometry (FTIR) and nuclear magnetic resonance (NMR) spectra are powerful tools that reveal information about surface functional groups and the structures of chemical compounds. As shown in Fig. 2B, the typical peak at 1717 cm^{-1} results from the stretching vibration of C=O, and the strong absorption at 1235 cm^{-1} can be attributed to the characteristic peaks of C–O–C stretching vibrations, demonstrating the abundant ester functional groups in the compound. The stretching vibration of C–N appears at 1074 cm^{-1}, and the peak at 2848 cm^{-1} is ascribed to the stretching vibration of aliphatic C–H from the quaternary ammonium (*32*). Solid-state ^{13}C cross-polarization/magic angle spinning (CP/MAS) NMR can characterize the molecular structure of highly insoluble q-PET unequivocally, according to the resulting chemical shifts. The isotropic resonances were assigned and labeled on the full spectrum shown in Fig. 2C. The resonance at 165.2 parts per million (ppm) is assigned to the carbonyl (C=O), and specific resonances at 130 to 134 ppm are attributed to the aromatic carbon. The characteristic peak of a methyl group ($-CH_3$) appears at 32.5 ppm with enhanced signal intensity because of the three methyl groups in the quaternary ammonium block (*33*, *34*). With smart design and control of the molecular structure, functional groups on the q-PET fiber with lithiophilic and anionphilic properties can efficiently assist the interlayer in regulating the distributions of ions under the electrical driving force.

From the macroscopic point of view, contact angle tests were used to investigate the affinity between the q-PET/Li composite electrode and ether-based electrolytes (Fig. 2D). The contact angle of ether-based electrolytes on the bare Li metal is 22.7°, suggesting that the lithium metal has poor wettability with ether-based electrolytes, which could cause the blocking of ionically conducting pathways (movie S1). In contrast, the contact angle of the q-PET/Li electrode (1 mA·hour cm^{-2} Li is predeposited to mimic the real state during cycling) is almost zero (movie S2). Because of its ultra-affinity with the electrolytes, the q-PET/Li composite electrode, instead of the bare lithium metal, can enhance the electrolyte uptake capability, which is beneficial to homogenize ion distributions in the vicinity of the anode and to reduce inner cell resistance.

Electrochemical performance of q-PET/Li composite anode

Lithium coulombic efficiency (CE) is an essential parameter to evaluate the reversibility of the lithium metal anode, which reflects the quantity of "dead" Li (electrically isolated Li metal from the substrate) in each cycle. Here, 1 mA·hour cm^{-2} of the Li metal is plated onto the Cu foil working electrode, followed by the complete stripping of the Li metal from the Cu foil at a cutoff voltage (1.0 V). The CE can be calculated according to the ratio of the Li stripping capacity to the Li plating capacity in each cycle. As presented in Fig. 3A and table S3, the q-PET/Li composite electrode exhibits higher lithium CE and longer cycling life span at all current densities. Under a current density of 1.0, 2.0, 5.0, or

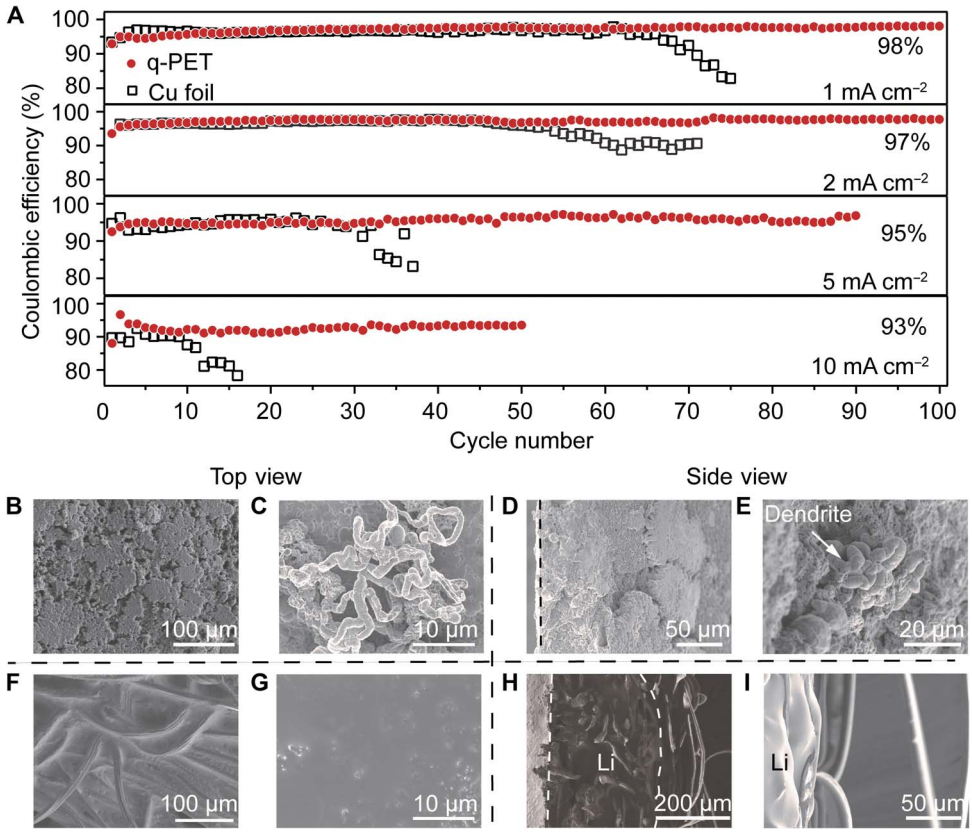

Fig. 3. Li CEs and anode surface morphology of Li/Cu cells with bare Li or q-PET/Li electrode at a current density of 2.0 mA cm^{-2}. (**A**) Comparison of Li CEs of cells with or without q-PET fabric at various current densities with the same areal capacity of 1.0 mA·hour cm^{-2}. Top-view (**B** and **C**) and cross-sectional (**D** and **E**) SEM images of dendritic Li deposition on bare Cu foil after 30 cycles. Top-view (**F** and **G**) and cross-sectional (**H** and **I**) SEM images of dendrite-free Li deposition on q-PET fiber–modified Cu foil after 30 cycles.

10.0 mA cm^{-2}, cells with the q-PET/Li electrode reveal improved lithium CE of 98, 97, 95, or 93%, respectively. At a low cycling rate of 1.0 mA cm^{-2}, cells with q-PET show stable cycling performance, maintaining an average Li CE of 98% for more than 300 cycles, whereas the Li CE of cells with the bare lithium metal drops below 90% after the initial 72 cycles (fig. S5A). When the current density is increased to 5 mA cm^{-2}, the Li CE of the q-PET/Li composite electrode still reaches 95% for more than 90 cycles, whereas the Li CE of the control electrode without the modification of q-PET drops below 90% after only 30 cycles. Even for a high Li areal capacity of 2.0 mA·hour cm^{-2}, the Li CE of the q-PET–modified cell maintains 97% over 70 cycles at 2.0 mA cm^{-2} (fig. S5B) or 95% over 50 cycles at 5.0 mA cm^{-2} (fig. S5C). After the cycle tests, the q-PET interlayer can maintain the original morphology, and there is no obvious dead Li (fig. S6). To further demonstrate the cation-anion regulation synergistic effect, a PET nonwoven fabric that contains only lithiophilic sites was chosen as a comparison (fig. S7, A and B). Compared with the bare Cu foil, the PET interlayer with abundant lithiophilic ester building block can deliver a stable Li CE and enhanced life span to some extent. Nevertheless, when lithiophilic and anionphilic sites are introduced into the skeleton of the molecular structure synchronously (q-PET), electrochemical performances of the q-PET/Li composite anode are improved drastically at all current densities (fig. S7C). These results suggest that functional groups on the q-PET fiber with lithiophilic and anionphilic sites can effectively enhance the use of the active anode material and decrease the generation of dead Li even at high current densities.

SEM analysis was performed to observe the differences in morphology of Li deposition after 30 cycles. Under a current density of 2.0 mA cm^{-2}, the Li deposition on the bare Cu foil exhibits mossy and dendritic structures (Fig. 3, B and D), with visible Li dendrites in a diameter of 5 μm (labeled in Fig. 3, C, top view, and E, side view). Endless dendrite proliferation will consume the Li metal and electrolytes continuously, leading to cell "dry-out" or safety risks. In comparison, dendrite-free morphology can be achieved using the q-PET/Li composite electrode via the cation-anion regulation property. From the top view, Li deposition exhibits a flat and dense morphology, without the observation of dendritic Li (Fig. 3, F and G). On the basis of the insulating property of the q-PET fiber, Li tends to deposit from the bottom of the fiber and fill up the q-PET matrix (Fig. 3, H and I). The dense deposition of lithium within the q-PET matrix can reduce the side reactions between the lithium metal and the electrolytes, which might be the underlying origin of the enhanced Li CE in Li/Cu cells. Driven by the strong interactions (Li ion with the ester group and $TFSI^-$ with quaternary ammonium), the q-PET fiber can absorb large amounts of ions. As a result, Li-ion flux around "hot spots" can be uniformed, and the concentration gradient of anions induced by the electric field can be relieved at the anode interface. Under this synergy, Li can still deposit smoothly on the q-PET–modified electrode at ultrahigh current densities (5.0 and 10.0 mA cm^{-2}) (fig. S8). Compared with the nonpolar PP separator, which directly contacts the bare lithium metal anode, the q-PET functional interlayer can delay or even prevent the Li dendrite proliferation.

Li/Li cells with ether-based electrolytes (containing 1% $LiNO_3$) were tested at different current densities to evaluate their voltage hysteresis and cycling stability. At a current density of 3 mA cm^{-2} (Fig. 4A, top), cells with the bare Li electrode exhibit a gradual increment in voltage hysteresis over 125 cycles, which is almost 10 times the initial voltage hysteresis. This can be attributed to the increasing internal resistance induced by the continuous breakdown and the reestablishment of SEI at the electrolyte/electrode interface. A sudden voltage drop was observed in the later cycles, suggesting an internal short circuit caused by Li dendrites. As expected, the q-PET–modified cells show lower voltage hysteresis and improved cycling stability over 1000 cycles (up to 650 hours) (fig. S9). The enlarged voltage profiles at specific times (30 and 80 hours) shown in Fig. 4A verify the stable cycling of the q-PET–modified cell with smooth voltage plateaus. When the current densities increased to 5 mA cm^{-2}, the q-PET–modified cells still show excellent electrochemical performances (Fig. 4A, middle). Stable cycling with low hysteresis of ~80 mV and a flat voltage plateau over 250 cycles was observed, whereas cells with the bare Li foil exhibit continuous increase in hysteresis from ~100 to ~230 mV over 52 cycles. Similarly, even at 10 mA cm^{-2} (Fig. 4A, bottom), the q-PET–modified cell can maintain good stability over 500 cycles (100 hours). These results reveal that the q-PET functional anode host can improve the interfacial stability and the reversibility of Li stripping/plating. When the areal capacity is increased to 2.0, 5.0, or 10.0 mA·hour cm^{-2}, huge volume expansion and uncontrolled proliferation of Li dendrites are expected to the control cells with early failure, whereas the q-PET–modified Li anode enhances the cycling stability and increases the cell lifetime (fig. S10). Electrochemical impedance spectroscopy was carried out using symmetric Li cells to analyze the inner resistance and interfacial stability after 1 (Fig. 4B) and 10 (Fig. 4C) cycles. The semicircle at the high-frequency range visually indicates the interfacial resistance and the charge transfer resistance at the electrolyte/electrode interface. After one cycle, cells with the bare Li metal anode exhibit a large interfacial resistance of ~170 ohms, which is almost five times that of cells with the q-PET/Li composite anode. After 10 cycles, the interfacial resistance for cells with the bare Li foil drops to ~65 ohms due to the decomposition of the fragile SEI layer and the formation of dendritic Li, which significantly increase the surface area of the Li anode. On the contrary, cells with the q-PET/Li composite anode show constantly low interfacial resistances of ~35 ohms after 1 cycle and ~30 ohms after 10 cycles. It can be explained by the enhanced wettability and electrode stability of the q-PET/Li composite anode. This result is consistent with the finding that cells with the q-PET–modified anode show lower hysteresis during stripping and plating.

To further evaluate the utility function of the q-PET functional anode host in LMBs, the q-PET/Li composite anode was paired with $LiFePO_4$ (LFP) or $Li_4Ti_5O_{12}$ (LTO) electrodes. Figure 5A shows the cycling performance of the Li/LFP half cell at a rate of 0.5 C. Cells using the Li/q-PET anode present a high initial capacity and maintain 137.1 mA·hour g^{-1} with a stable CE after 150 cycles. In contrast, the

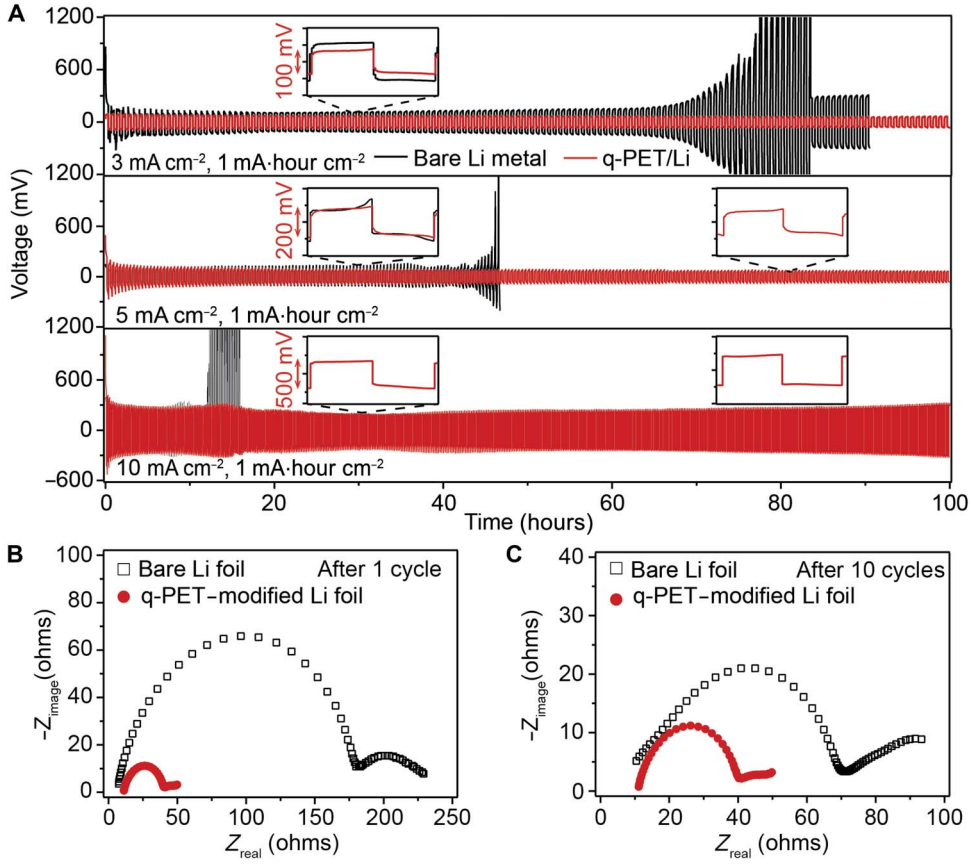

Fig. 4. Electrochemical performance of symmetric cells with bare Li (black) or q-PET/Li electrode (red). (**A**) The total capacity is fixed at 1 mA·hour cm^{-2}. Voltage profiles of symmetric cells at various current densities of 3 mA cm^{-2} (top), 5 mA cm^{-2} (middle), and 10 mA cm^{-2} (bottom). (**B** and **C**) Nyquist plot of the impedance spectra after the 1st (B) and 10th (C) cycle at a current density of 3 mA cm^{-2}.

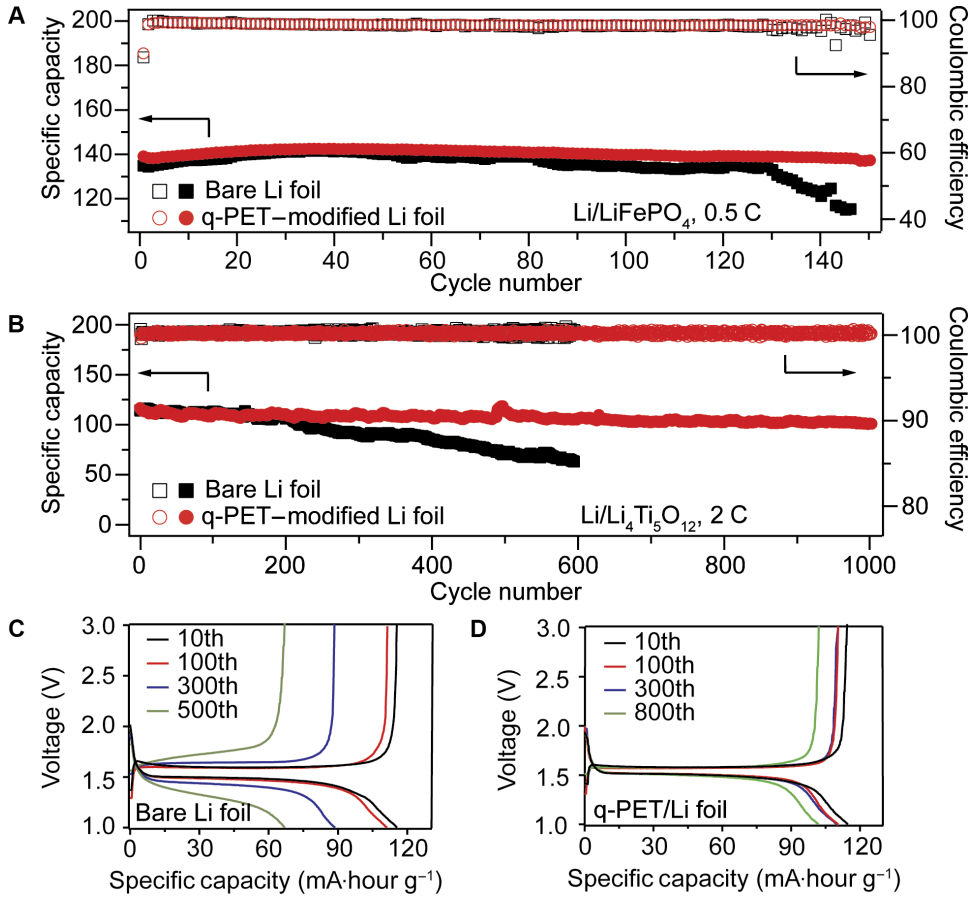

Fig. 5. Electrochemical performance of half cells with q-PET/Li composite anode. (**A**) Long-term cycling performance of Li/LFP half cell at 0.5 C with bare Li (black) or q-PET/Li electrode (red). (**B**) Long-term cycling performance of Li/LTO half cell at 2 C with or without q-PET. (**C**) Charge-discharge profiles of the Li/LTO cell with the bare Li foil at 2 C. (**D**) Charge-discharge profiles of the Li/LTO cell with the q-PET–modified Li foil at 2 C.

capacity of cells with the bare Li electrode degrades after 80 cycles and maintains only 105.6 mA·hour g^{-1} at 150 cycles, and the overall overpotential grows significantly during cycling (fig. S11). We also used the Li/q-PET anode with the zero-strain LTO cathode. At a high rate of 2 C, cells with the q-PET–modified anode show superior cycling life, achieving stable discharge capacity with a steady CE of 99.9% for 1000 cycles without significant degradation, whereas cells with the bare Li foil degraded harshly after 208 cycles (Fig. 5B). It can be seen from Fig. 5C that the capacity of cells without the q-PET interlayer fades quickly and the overall overpotential grows significantly during cycling, which can be caused by the uncontrollable proliferation of Li dendrites and the thickened SEI. In contrast, modified cells exhibit almost unchanged overpotential and flat voltage plateau over 1000 cycles (Fig. 5D). The q-PET interlayer can also improve the initial CE of both Li/LFP and Li/LTO half cells slightly (fig. S12). These results suggest that the q-PET functional anode host can dramatically improve the cyclability and stability of LMBs.

DISCUSSION

The cation-anion regulation synergistic effect is proposed as a novel concept to promote dendrite-free Li deposition during cycling. q-PET with lithiophilic and anionphilic sites in the skeleton of its molecular structures shows strong interactions with ions in the electrolytes, which is confirmed by DFT calculations. Lithiophilic ester groups can uniform Li-ion flux at the electrolyte/electrode interface, protecting the enhanced local Li-ion flux from the tip effect, and anionphilic quaternary ammonium can attract anions at the interface, avoiding the space charge induced by a local deficit of anions. Under the synergistic effect, cells with the q-PET/Li composite anode exhibit remarkable cyclability and stability. Under a current density of 1.0, 2.0, 5.0, or 10.0 mA cm^{-2}, the q-PET–modified cells show extended life span and improved CE of 98, 97, 95, or 93%, respectively. Under a current density of 3 mA cm^{-2}, the q-PET anode host provides up to sixfold improvement in cell lifetime (up to 650 hours), proving the vital role of the q-PET interlayer on regulating the Li deposits. Ultralong cycling life span was realized using the q-PET functional anode host in Li/LTO half cells, implying the huge potential for practical applications in LMBs. This novel tactic can also be applied to other high-energy battery systems involving Na, Al, Mg, Zn, and so forth.

MATERIALS AND METHODS

Computational details

DFT calculations were carried out using the Vienna Ab initio Simulation Package (version 5.4.1). The exchange-correlation interactions were described by the Perdew-Burke-Ernzerhof (PBE) functional (*35*). Consistently, we used the PBE version of the projector augmented-wave

method potential data set to describe electron-nucleus interactions (*36*, *37*). We used the plane wave basis with a cutoff energy of 500 eV. A cubic vacuum box with a side length of 45 Å was used for all the calculations along with a single Γ point for the *k*-point sampling. The atomic positions were optimized until the energy and force satisfied their convergence criteria of 10^{-5} and 0.03 eV/Å, respectively.

Materials

The Li foil was purchased from Sinopharm Chemical Reagent Co. Ltd. and was polished by a drawknife until the surface was metallic shiny. The q-PET nonwoven fabric was purchased from WARD GmbH. Copper foils and LFP cathodes (active material surface density, 120 g m^{-2}; total thickness, 83 μm) were bought from Shenzhen Kejing Star Technology Co. Ltd. The LTO cathode (LTO/carbon black/polyvinylidene difluoride = 8:1:1 by weight ratio) was prepared using a blade-casting method. The electrolyte used in Li/Cu cells was 1 M LiTFSI in dioxolane/dimethoxyethane (DOL/DME) (1:1 by volume) with 2 wt % $LiNO_3$ additive. The electrolyte used in Li/Li symmetrical cells was 1 M LiTFSI in DOL/DME (1:1 by volume) with 1 wt % $LiNO_3$ additive. The electrolyte used in Li/LFP and Li/LTO half cells was 1 M lithium hexafluorophosphate ($LiPF_6$) in ethylene carbonate/diethyl carbonate (EC/DEC) (1:1 by volume), and all the electrolytes were purchased from DodoChem. The separator used was Celgard 2400 (25-μm monolayer PP).

Electrochemical measurements

Coin cells, type 2032, were assembled in an Ar-filled glove box with O_2 and H_2O content below 0.1 ppm. The LAND electrochemical testing system and Solartron Analytical Electrochemical Workstation were used for the electrochemical measurements. To evaluate the Li CE, we used the Cu foil (1 cm^2) covered with the q-PET fabric (1 cm^2) as the modified working electrode, the Li foil as the counter/reference electrode, and 60-μl electrolyte for each cell. The cells were cycled at 0 to 1 V for one cycle (for SEI formation, no Li deposition). Then, a fixed amount of lithium (1 or 2 mA·hour cm^{-2}) was plated onto the current collector and stripped back by a cutoff voltage (1.0 V). Li/Li symmetrical cells were cycled at 3 mA cm^{-2} for 20 min, 5 mA cm^{-2} for 12 min, and 10 mA cm^{-2} for 6 min. The Li/LFP cells were cycled within the potential range of 2.2 to 4.2 V (versus Li/Li^+) at 0.2 C for one cycle and cycled at 0.5 C for the rest of the cycles. The Li/LTO half cells were cycled within the potential range of 1.0 to 3.0 V (versus Li/Li^+) at 2 C at room temperature.

Characterizations

The FTIR spectrum was measured using Thermo iS50. Solid-state ^{13}C CP/MAS NMR spectra were measured using a Bruker Avance HD 400 MHz spectrometer. The ^{13}C signals were referenced to the methylene signal of adamantane at 38.5 ppm. The contact angle was measured with Dataphysics OCA50AF, and a 3.0-μl droplet of ether-based electrolytes (1 M LiTFSI DOL/DME = 1:1; 2% $LiNO_3$) was used in the experiment. SEM measurements were conducted on a field emission SEM (Hitachi SU8000 FE-SEM) at 5 kV. Optical microscopy analyses were conducted on a Nikon DS TI-FL.

SUPPLEMENTARY MATERIALS

Supplementary material for this article is available at http://advances.sciencemag.org/cgi/content/full/4/2/eaar4410/DC1

fig. S1. Sketch of the structures of PP separator and Li atom after geometry optimizations.
fig. S2. Images of q-PET nonwoven fabric.
fig. S3. SEM and elemental mapping images showing the homogenous distribution of C, N, and O in the q-PET fiber.
fig. S4. EDX spectrum under SEM mode.
fig. S5. Cycling performances of Li/Cu cells.
fig. S6. Digital picture of q-PET interlayer after 30 cycles.
fig. S7. Effectiveness of lithiophilic effect only.
fig. S8. SEM images of Li deposition on q-PET fiber–modified electrodes after 10 cycles.
fig. S9. Galvanostatic cycling performance of symmetrical cells.
fig. S10. Galvanostatic cycling performance of symmetrical cells at 5 mA cm^{-2} with high areal capacities of 2, 5, or 10 mA·hour cm^{-2}.
fig. S11. Charge-discharge profiles of the Li/LFP cells at different cycles.
fig. S12. Voltage profiles of Li/LFP and Li/LTO half cells with or without q-PET (first cycle).
table S1. Binding energies using DFT calculations.
table S2. Elemental analysis (Dumas combustion).
table S3. Li CE of q-PET–modified cells compared with other state-of-the-art modifications.
movie S1. Shape of a droplet (ether-based electrolyte) on the bare lithium foil.
movie S2. Spreading behavior of a droplet (ether-based electrolyte) on the q-PET/Li composite anode.
References (*38*–*45*)

REFERENCES AND NOTES

1. X. B. Cheng, R. Zhang, C. Z. Zhao, Q. Zhang, Toward safe lithium metal anode in rechargeable batteries: A review. *Chem. Rev.* **117**, 10403–10473 (2017).
2. Y. Guo, H. Li, T. Zhai, Reviving lithium-metal anodes for next-generation high-energy batteries. *Adv. Mater.* **29**, 1700007 (2017).
3. M. D. Tikekar, S. Choudhury, Z. Tu, L. A. Archer, Design principles for electrolytes and interfaces for stable lithium-metal batteries. *Nat. Energy* **1**, 16114 (2016).
4. D. Lin, Y. Liu, Y. Cui, Reviving the lithium metal anode for high-energy batteries. *Nat. Nanotechnol.* **12**, 194–206 (2017).
5. J.-M. Tarascon, M. Armand, Issues and challenges facing rechargeable lithium batteries. *Nature* **414**, 359–367 (2001).
6. D. Lin, Y. Liu, Z. Liang, H.-W. Lee, J. Sun, H. Wang, K. Yan, J. Xie, Y. Cui, Layered reduced graphene oxide with nanoscale interlayer gaps as a stable host for lithium metal anodes. *Nat. Nanotechnol.* **11**, 626–632 (2016).
7. Q. Li, S. Tan, L. Li, Y. Lu, Y. He, Understanding the molecular mechanism of pulse current charging for stable lithium-metal batteries. *Sci. Adv.* **3**, e1701246 (2017).
8. S. Choudhury, Z. Tu, S. Stalin, D. Vu, K. Fawole, D. Gunceler, R. Sundararaman, L. A. Archer, Electroless formation of hybrid lithium anodes for fast interfacial ion transport. *Angew. Chem. Int. Ed.* **56**, 13070–13077 (2017).
9. P. Bai, J. Li, F. R. Brushett, M. Z. Bazant, Transition of lithium growth mechanisms in liquid electrolytes. *Energy Environ. Sci.* **9**, 3221–3229 (2016).
10. Z. Tu, P. Nath, Y. Lu, M. D. Tikekar, L. A. Archer, Nanostructured electrolytes for stable lithium electrodeposition in secondary batteries. *Acc. Chem. Res.* **48**, 2947–2956 (2015).
11. C. Brissot, M. Rosso, J.-N. Chazalviel, S. Lascaud, Dendritic growth mechanisms in lithium/polymer cells. *J. Power Sources* **81–82**, 925–929 (1999).
12. L. Enze, The application of a surface charge density distribution function to the solution of boundary value problems. *J. Phys. D Appl. Phys.* **20**, 1609 (1987).
13. C. Monroe, J. Newman, Dendrite growth in lithium/polymer systems. A propagation model for liquid electrolytes under galvanostatic conditions. *J. Electrochem. Soc.* **150**, A1377–A1384 (2003).
14. A. Kushima, K. P. So, C. Su, P. Bai, N. Kuriyama, T. Maebashi, Y. Fujiwara, M. Z. Bazant, J. Li, Liquid cell transmission electron microscopy observation of lithium metal growth and dissolution: Root growth, dead lithium and lithium flotsams. *Nano Energy* **32**, 271–279 (2017).
15. M. Rosso, T. Gobron, C. Brissot, J.-N. Chazalviel, S. Lascaud, Onset of dendritic growth in lithium/polymer cells. *J. Power Sources* **97–98**, 804–806 (2001).
16. J.-N. Chazalviel, Electrochemical aspects of the generation of ramified metallic electrodeposits. *Phys. Rev. A* **42**, 7355–7367 (1990).
17. Z. Liang, G. Zheng, C. Liu, N. Liu, W. Li, K. Yan, H. Yao, P. C. Hsu, S. Chu, Y. Cui, Polymer nanofiber-guided uniform lithium deposition for battery electrodes. *Nano Lett.* **15**, 2910–2916 (2015).
18. X.-B. Cheng, T.-Z. Hou, R. Zhang, H.-J. Peng, C.-Z. Zhao, J.-Q. Huang, Q. Zhang, Dendrite-free lithium deposition induced by uniformly distributed lithium ions for efficient lithium metal batteries. *Adv. Mater.* **28**, 2888–2895 (2016).
19. M. D. Tikekar, L. A. Archer, D. L. Koch, Stability analysis of electrodeposition across a structured electrolyte with immobilized anions. *J. Electrochem. Soc.* **161**, A847–A855 (2014).
20. M. D. Tikekar, L. A. Archer, D. L. Koch, Stabilizing electrodeposition in elastic solid electrolytes containing immobilized anions. *Sci. Adv.* **2**, e1600320 (2016).
21. Y. Lu, M. Tikekar, R. Mohanty, K. Hendrickson, L. Ma, L. A. Archer, Stable cycling of lithium metal batteries using high transference number electrolytes. *Adv. Energy Mater.* **5**, 1402073 (2015).

22. Y. Lu, S. K. Das, S. S. Moganty, L. A. Archer, Ionic liquid-nanoparticle hybrid electrolytes and their application in secondary lithium-metal batteries. *Adv. Mater.* **24**, 4430–4435 (2012).
23. Y. Lu, K. Korf, Y. Kambe, Z. Tu, L. A. Archer, Ionic-liquid–nanoparticle hybrid electrolytes: Applications in lithium metal batteries. *Angew. Chem. Int. Ed.* **53**, 488–492 (2014).
24. S. S. Zhang, Role of $LiNO_3$ in rechargeable lithium/sulfur battery. *Electrochim. Acta* **70**, 344–348 (2012).
25. Y. Lu, Z. Tu, L. A. Archer, Stable lithium electrodeposition in liquid and nanoporous solid electrolytes. *Nat. Mater.* **13**, 961–969 (2014).
26. L. Fan, H. L. Zhuang, L. Gao, Y. Lu, L. A. Archer, Regulating Li deposition at artificial solid electrolyte interphases. *J. Mater. Chem. A* **5**, 3483–3492 (2017).
27. Y. Lu, Z. Tu, J. Shu, L. A. Archer, Stable lithium electrodeposition in salt-reinforced electrolytes. *J. Power Sources* **279**, 413–418 (2015).
28. W. Li, H. Yao, K. Yan, G. Zheng, Z. Liang, Y.-M. Chiang, Y. Cui, The synergetic effect of lithium polysulfide and lithium nitrate to prevent lithium dendrite growth. *Nat. Commun.* **6**, 7436 (2015).
29. X.-B. Cheng, C. Yan, X. Chen, C. Guan, J.-Q. Huang, H.-J. Peng, R. Zhang, S.-T. Yang, Q. Zhang, Implantable solid electrolyte interphase in lithium-metal batteries. *Chem* **2**, 258–270 (2017).
30. B. Su, W. Guo, L. Jiang, Learning from nature: Binary cooperative complementary nanomaterials. *Small* **11**, 1072–1096 (2015).
31. Y. Lu, S. S. Moganty, J. L. Schaefer, L. A. Archer, Ionic liquid-nanoparticle hybrid electrolytes. *J. Mater. Chem.* **22**, 4066–4072 (2012).
32. N. H. Mohamed, T. Bahners, A. Wego, J. S. Gutmann, M. Ulbricht, Surface modification of poly(ethylene terephthalate) fabric via photo-chemical reaction of dimethylaminopropyl methacrylamide. *Appl. Surf. Sci.* **259**, 261–269 (2012).
33. C. A. Fyfe, J. R. Lyerla, W. Volksen, C. S. Yannoni, High-resolution carbon-13 nuclear magnetic resonance studies of polymers in the solid state. Aromatic polyesters. *Macromolecules* **12**, 757–761 (1979).
34. D. L. Tzou, P. Desai, A. S. Abhiraman, T.-H. Huang, NMR studies of the structural development of high-speed melt-spun poly (ethylene terephthalate) fibers. *J. Polym. Sci. B* **29**, 49–56 (1991).
35. J. P. Perdew, K. Burke, M. Ernzerhof, Generalized gradient approximation made simple. *Phys. Rev. Lett.* **77**, 3865 (1996).
36. P. E. Blöchl, Projector augmented-wave method. *Phys. Rev. B* **50**, 17953 (1994).
37. G. Kresse, D. Joubert, From ultrasoft pseudopotentials to the projector augmented-wave method. *Phys. Rev. B* **59**, 1758–1775 (1999).
38. X.-Q. Zhang, X. Chen, R. Xu, X.-B. Cheng, H.-J. Peng, R. Zhang, J.-Q. Huang, Q. Zhang, Columnar lithium metal anodes. *Angew. Chem. Int. Ed.* **56**, 14207–14211 (2017).
39. Q. Li, S. Zhu, Y. Lu, 3D porous Cu current collector/Li-metal composite anode for stable lithium-metal batteries. *Adv. Funct. Mater.* **27**, 1606422 (2017).
40. K. Liu, A. Pei, H. R. Lee, B. Kong, N. Liu, D. Lin, Y. Liu, C. Liu, P.-c. Hsu, Z. Bao, Y. Cui, Lithium metal anodes with an adaptive "solid–liquid" interfacial protective layer. *J. Am. Chem. Soc.* **139**, 4815–4820 (2017).
41. W. Liu, D. Lin, A. Pei, Y. Cui, Stabilizing lithium metal anodes by uniform Li-ion flux distribution in nanochannel confinement. *J. Am. Chem. Soc.* **138**, 15443–15450 (2016).
42. R. Zhang, X.-R. Chen, X. Chen, X.-B. Cheng, X.-Q. Zhang, C. Yan, Q. Zhang, Lithiophilic sites in doped graphene guide uniform lithium nucleation for dendrite-free lithium metal anodes. *Angew. Chem. Int. Ed.* **56**, 7764–7768 (2017).
43. Y. Liu, D. Lin, P. Y. Yuen, K. Liu, J. Xie, R. H. Dauskardt, Y. Cui, An artificial solid electrolyte interphase with high Li-ion conductivity, mechanical strength, and flexibility for stable lithium metal anodes. *Adv. Mater.* **29**, 1605531 (2017).
44. B. Zhu, Y. Jin, X. Hu, Q. Zheng, S. Zhang, Q. Wang, J. Zhu, Poly(dimethylsiloxane) thin film as a stable interfacial layer for high-performance lithium-metal battery anodes. *Adv. Mater.* **29**, 1603755 (2017).
45. J. Luo, C.-C. Fang, N.-L. Wu, High polarity poly(vinylidene difluoride) thin coating for dendrite-free and high-performance lithium metal anodes. *Adv. Energy Mater.* **8**, 1701482 (2018).

Acknowledgments: We thank F. Chen (Department of Chemistry, Zhejiang University) for SEM analysis. We also thank Y. Fei (College of Civil Engineering and Architecture, Zhejiang University) for 3D graphing. **Funding:** This work was supported by the National Key R&D Program of China (grant 2016YFA0202900), Natural Science Foundation of China (grant 21676242), and State Key Laboratory of Chemical Engineering (grant SKL-ChE-17D01). This research also used computational resources of the Texas Advanced Computing Center under contract no. TG-DMR170070. H.L.Z. thanks the start-up funds from Arizona State University.
Author contributions: W.Z., H.L.Z., and Y.L. conceived the idea, designed the experiments, and wrote the manuscript. W.Z. performed the experimental work and analyzed the results with the help of L.F. L.G. conducted the MAS-NMR experiments and analyzed the results with the help of W.Z. H.L.Z. conducted the simulation work. **Competing interests:** The authors declare that they have no competing interests. **Data and materials availability:** All data needed to evaluate the conclusions in the paper are present in the paper and/or the Supplementary Materials. Additional data related to this paper may be requested from the authors.

Submitted 8 November 2017
Accepted 25 January 2018
Published 23 February 2018
10.1126/sciadv.aar4410

Citation: W. Zhang, H. L. Zhuang, L. Fan, L. Gao, Y. Lu, A "cation-anion regulation" synergistic anode host for dendrite-free lithium metal batteries. *Sci. Adv.* **4**, eaar4410 (2018).